JOINT INSTITUTE FOR NUCLEAR RESEARCH

Flerov Laboratory of Nuclear Reactions

FINAL REPORT ON THE INTEREST PROGRAMME

"Production and Spectroscopic Investigation of New Neutron Rich Isotopes Near the Neutron N=126 Shell Closure Using the Multi-nucleon Transfer Reactions"

Supervisor:
Mr. Viacheslav Vedeneev

Student:
Nishant Gaurav
Indian Institute of Science Education and Research (IISER)
Kolkata, India
ng19ms003@iiserkol.ac.in

Participation Period:
February 14 – April 10, 2022

Wave 6
Dubna, Russia

Abstract

Mass Analyzer of Super Heavy Atoms (MASHA) with the resolving power of approx. 1700 uses Isotope Separation On-Line (ISOL) methods for the separation of reaction products of multi-nucleon transfer reactions. The MASHA setup at Flerov Laboratory of Nuclear Reactions (FLNR) at Joint Institute for Nuclear Research (JINR), Dubna, Russia, is based on the beamline of the Cyclotron U-400M. The data collected by MASHA setup at FLNR for complete fusion reactions of ^{40}Ar+^{148}Sm, ^{40}Ar+^{166}Er, and multinucleon transfer reaction of ^{48}Ca+^{242}Pu near the neutron N=126 shell closure is analyzed using Origin Software, and the corresponding heatmap for α-decay energy profile has also been studied.

Introduction

The set of isotopes of superheavy elements (SHE), which is located at the island of stability in the nuclear stability map, are considered to live longer as compared to other isotopes of these elements. MASHA at Flerov Laboratory of Nuclear Reactions (FLNR) at Joint Institute of Nuclear Research (JINR), Dubna, Russia, is a mass spectrometer that works in a large variety of masses upto 450 a.m.u. and is used for the investigations of various physical properties of superheavy elements. The Isotope Separator Online (ISOL) technique is used for the separation of the products of the reactions, and they are detected by a multi-channel Si detector based on the focal of the MASHA apparatus.

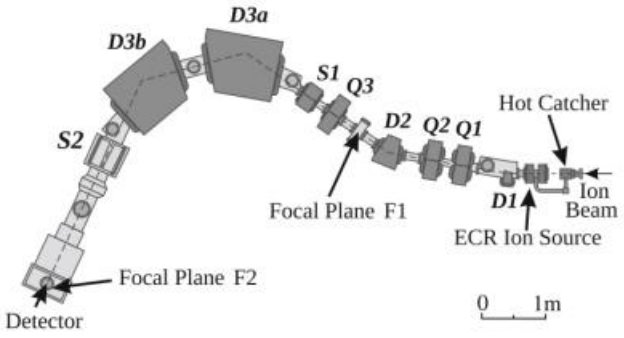

: Layout of MASHA spectrometer

The setup consists of an ion-optical layout, ECR ion source, hot catcher, target box, detectors, and control system. The ion beam passes through the rotating target with the energy of the order of a hundred MeV in total (about 5-7 MeV/nucleon), and then inside the hot catcher, the reaction products and the

unreacted beam is stopped. The target system represents a block of rotating targets assembled into cassettes rotating at frequency of about 25 Hz, and the rotating target is used to yield higher efficiency and heat distribution. The ion beam collides with the target, and then the reaction products are stopped in a catcher. The beam intensity is measured by the Faraday cup and the pick-up detector that has been installed. The pick-up sensor is an electrically isolated disc with a hole at the center, allowing the products to pass it and gather secondary electrons emitted from the target. The reaction products, after being emitted from the target, pass through the separating foil and stop in a graphite foil heats up to 1800-2000K. The nuclear reaction products diffuse in the form of atoms from the graphite into the vacuum volume of the hot catcher. Moving along the vacuum pipe, they reach the ECR ion source. Neutral atoms diffuse out from the poly-graphene structure of the hot-catcher, and with the help of an electron cyclotron resonance (ECR) ion source, it gets ionized to Q = +1 to the energy of 38 keV by applying the ultra-high frequency of 2.45GHz. Even for the noble gases, the ionization efficiency of 90% is obtained. In the system of a magneto-optical mass-to-charge ratio analyzer, the actual mass separation takes place, which is composed of four dipole magnets (D1, D2, D3a, D3b), three quadrupole lenses (Q1, Q2, Q3), and two sextupole lenses (S1, S2). The next step is focusing the ions of interest on the focal plane, and with the help of a multi-channel Si detector, it gets detected. The front panel of the silicon detector has 192 strips with a pitch of 1.25 mm covered by copper with an energy resolution of about 30 keV. The multi-strip silicon structure is fixed on the surface of the glass-cloth laminate and has an area of 240x35 mm^2. All detectors have a thickness of about 300 μm. They are used to determine the energies of the α-emission and the spontaneous fission. Furthermore, four additional detector panels have been installed on the top-bottom and right-left sides of the front detector panel to increase the geometrical efficiency of α-decay products. This allows the detection of 90% of the α-particles.

Methods

In the first step, we will plot the data obtained from the reactions of $^{40}Ar + ^{148}Sm$, $^{40}Ar + ^{166}Er$, and $^{48}Ca + ^{242}Pu$ at MASHA setup using OriginPro software and fit the graph using peak analyzer tools to get the product isotope from its decay energy and alpha branching ratio for the exact nucleus for each of the reaction data.

The second task is to construct the heatmap for the three reactions profile mentioned above and calibrate the y-axis with the E(alpha decay) = a*x+b formula to get the alpha decay energy value for different isotopes.

Results

(i) $^{40}Ar + ^{148}Sm$:

Peak Index	Peak Type	Area Intg	FWHM	Max Height	Center Grvty	Area IntgP
1	Gaussian	1916.35172	11.56166	255.19662	5728.59606	4.17892
2	Gaussian	6.33E-11	14.10059	137.13862	5771.32938	1.38036E-13
3	Gaussian	43941.21357	13.45196	643.81958	6122.73512	95.82108
4	Gaussian	0	0.29144	115	7700	0

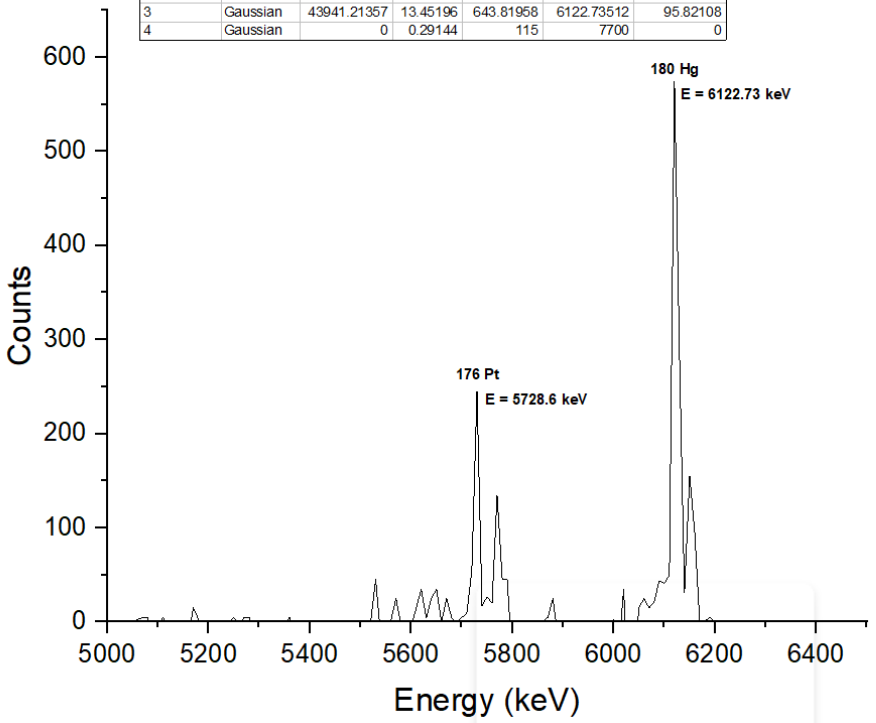

: 1D spectra of ^{180}Hg isotope

Peak Index	Peak Type	Area Intg	FWHM	Max Height	Center Grvty	Area IntgP
1	Gaussian	0	7.47734	18579.9523	5990.52826	--

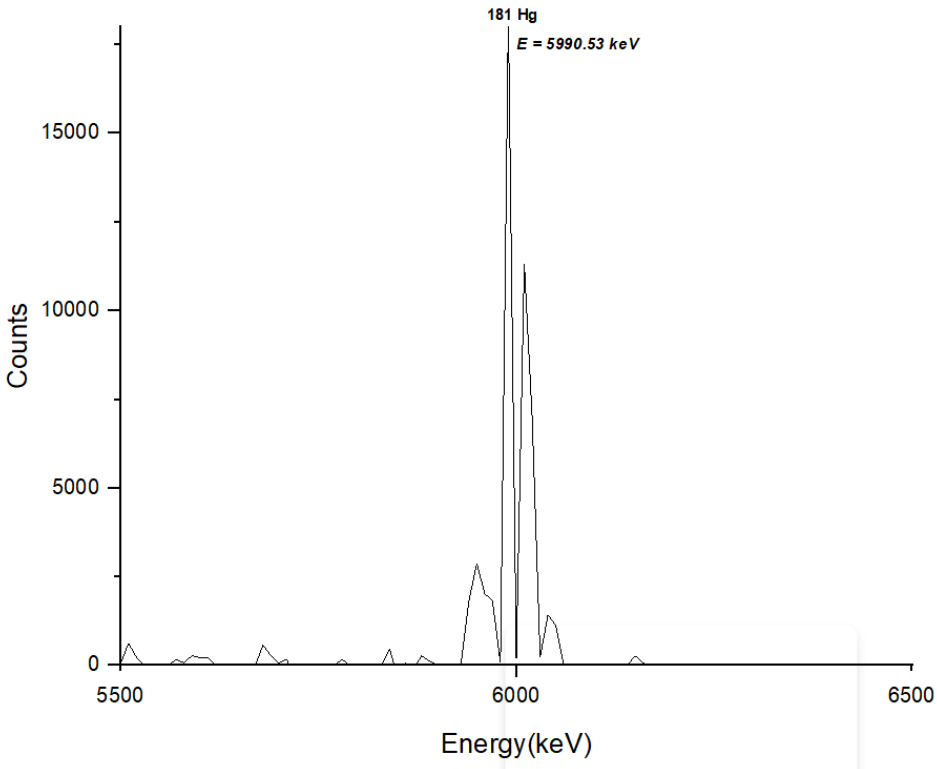

: 1D spectra of ^{181}Hg isotope

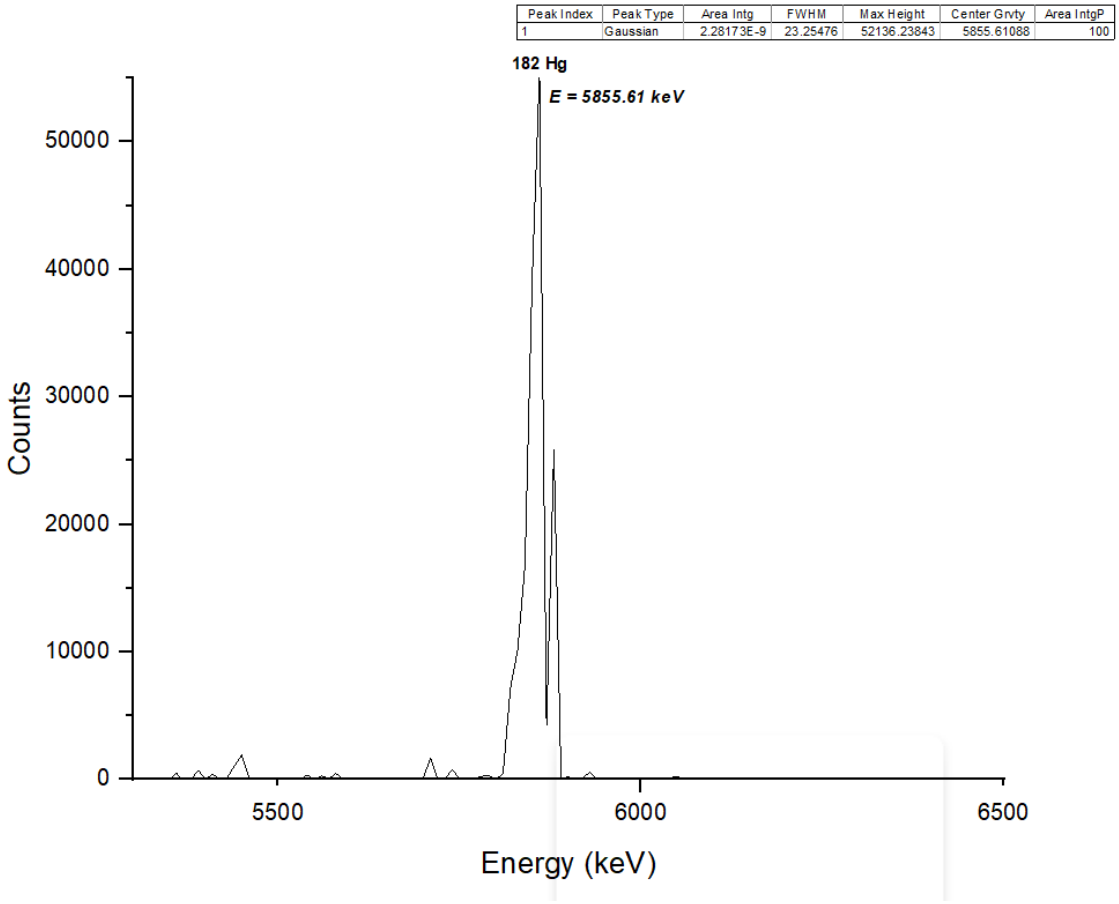

: 1D spectra of ^{182}Hg isotope

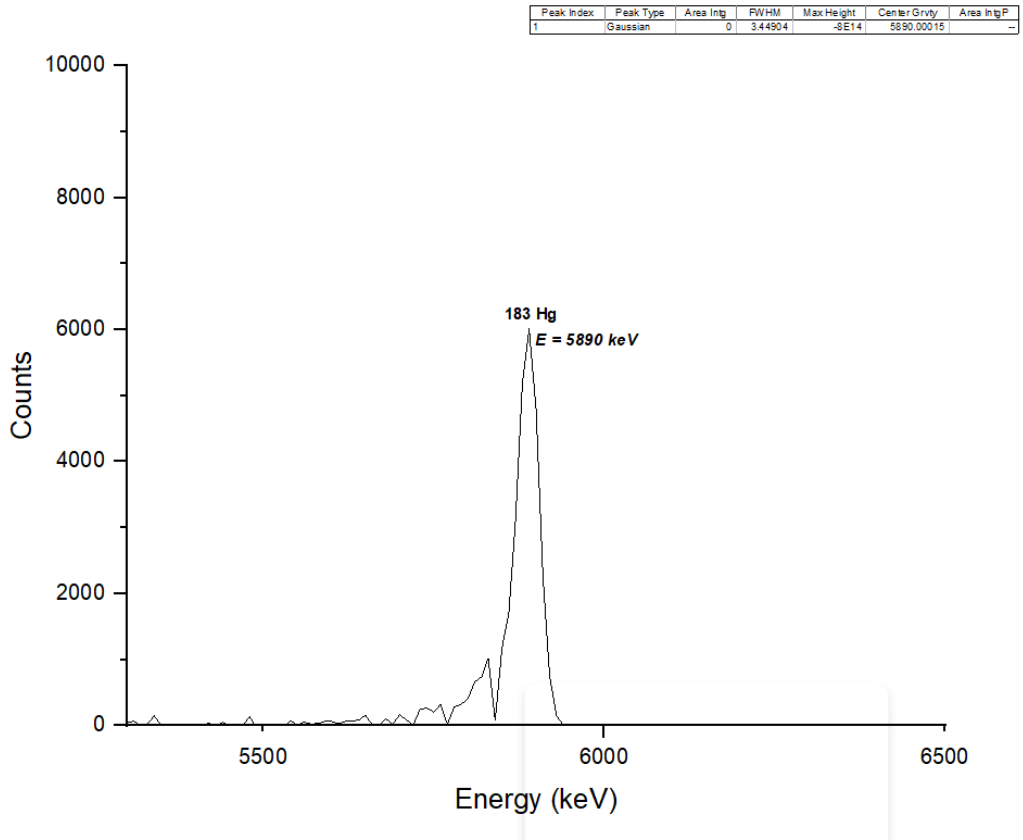

: 1D spectra of ^{183}Hg isotope

Peak Index	Peak Type	Area Intg	FWHM	Max Height	Center Grvty	Area IntgP
1	Gaussian	39050.99399	36.94086	196.92866	5531.76161	99.99998
2	Gaussian	-0.00905	18.69409	-48.37199	5989.46026	-2.31715E-5

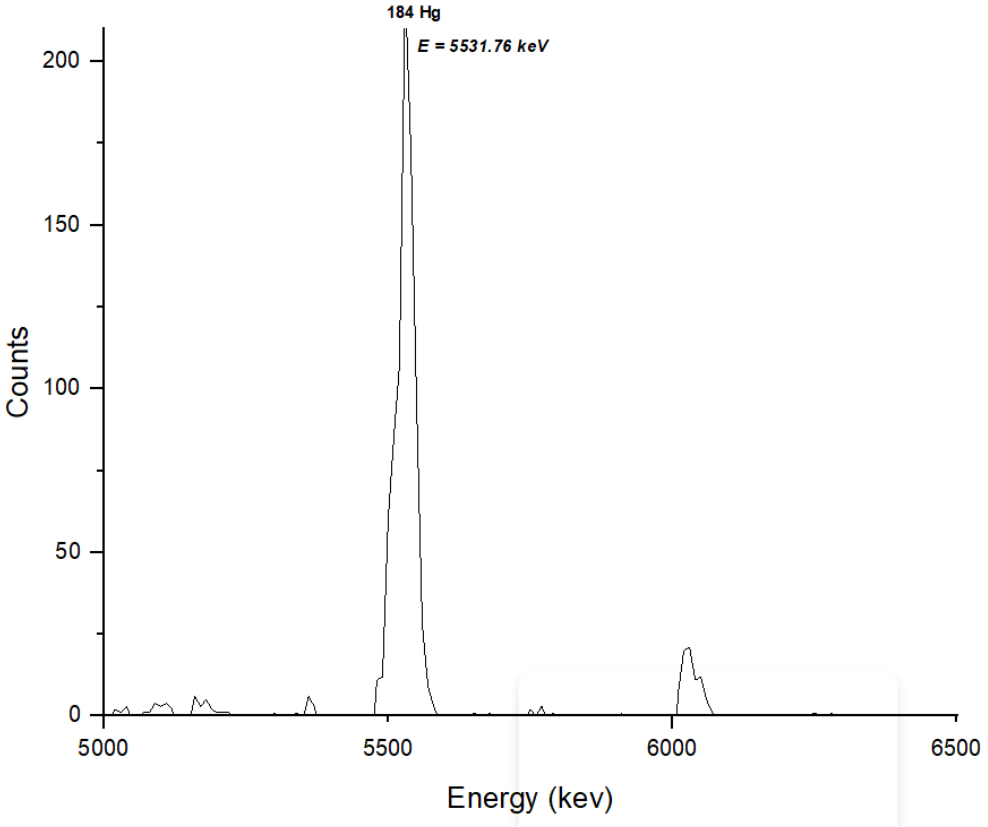

: 1D spectra of ^{184}Hg isotope

Peak Index	Peak Type	Area Intg	FWHM	Max Height	Center Grvty	Area IntgP
1	Gaussian	3.29998E-11	33.8516	1544.22578	5646.41155	100

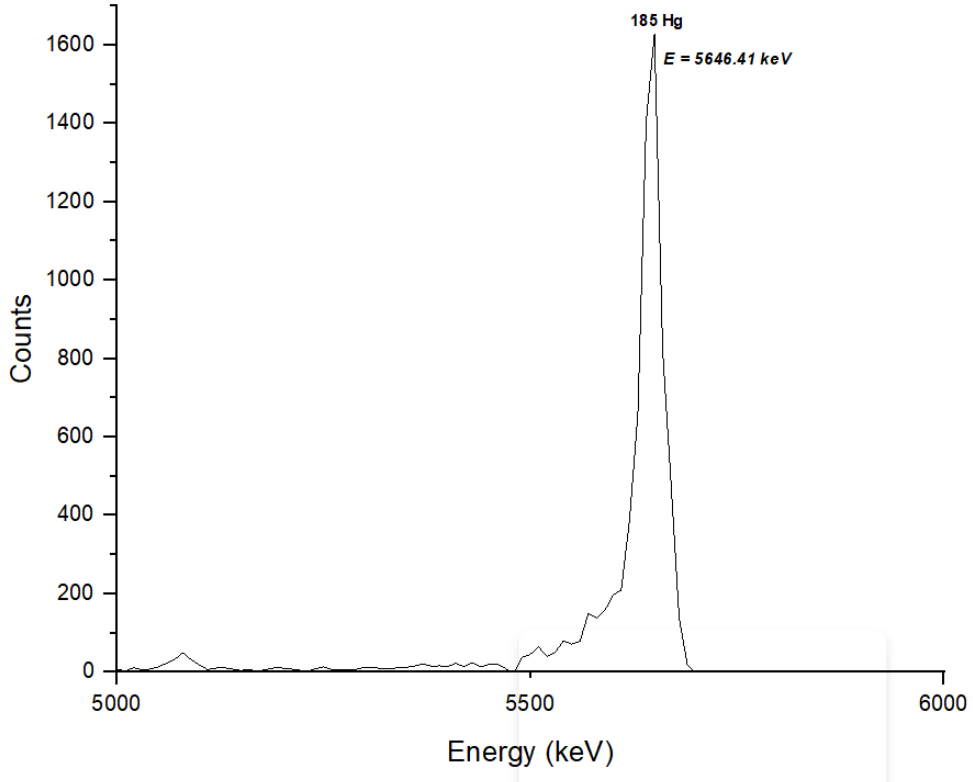

: 1D spectra of ^{185}Hg isotope

Heatmap of alpha decay energy of $^{40}Ar + ^{148}Sm$-

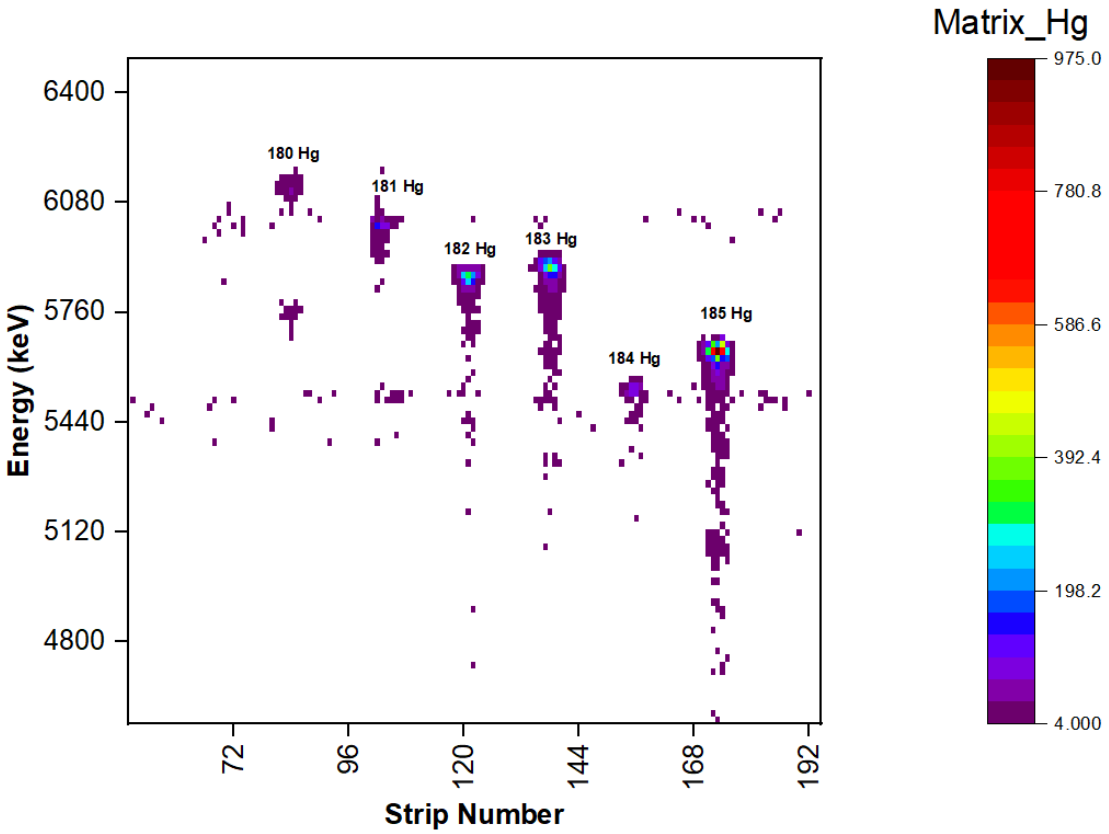

: 2D heatmap of alpha decay energies of $^{180\text{-}185}Hg$ isotopes

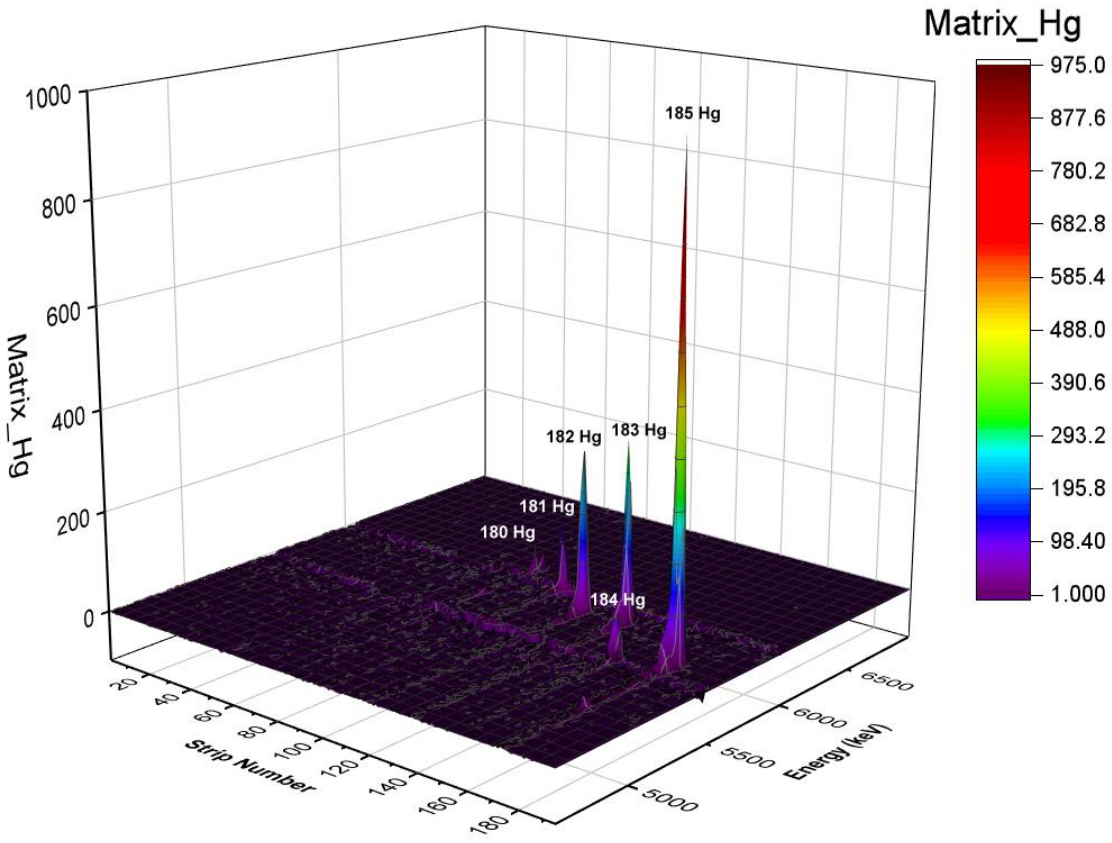

: 3D heatmap of alpha decay energies of $^{180\text{-}185}Hg$ isotopes

(ii) $^{40}Ar + {}^{166}Er$:

Peak Index	Peak Type	Area Intg	FWHM	Max Height	Center Grvty	Area IntgP
1	Gaussian	77744.56268	227.1093	321.58272	6309.58593	50.68629
2	Gaussian	4750.298	39.89251	815.17543	6374.38758	3.097
3	Gaussian	70888.93433	83.82797	1387.10384	6745.94358	46.2167

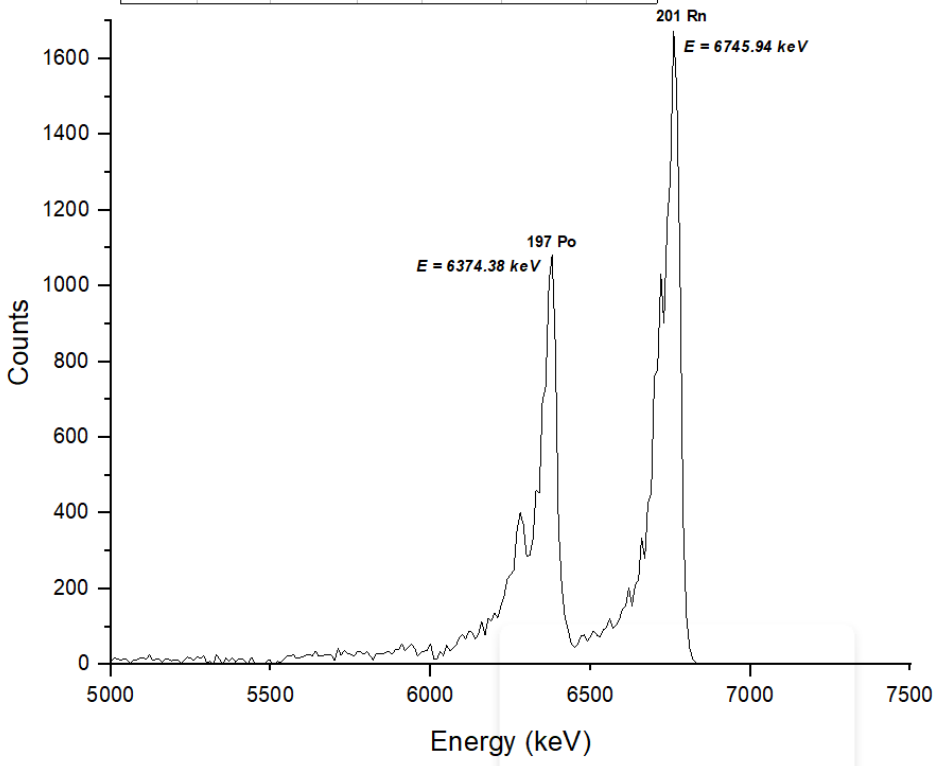

: 1D spectra of ^{201}Rn isotope

Peak Index	Peak Type	Area Intg	FWHM	Max Height	Center Grvty	Area IntgP
1	Gaussian	138196.94801	66.22731	751.958	6166.7397	96.11176
2	Gaussian	5590.80753	47.04797	1827.77632	6622.89093	3.88824

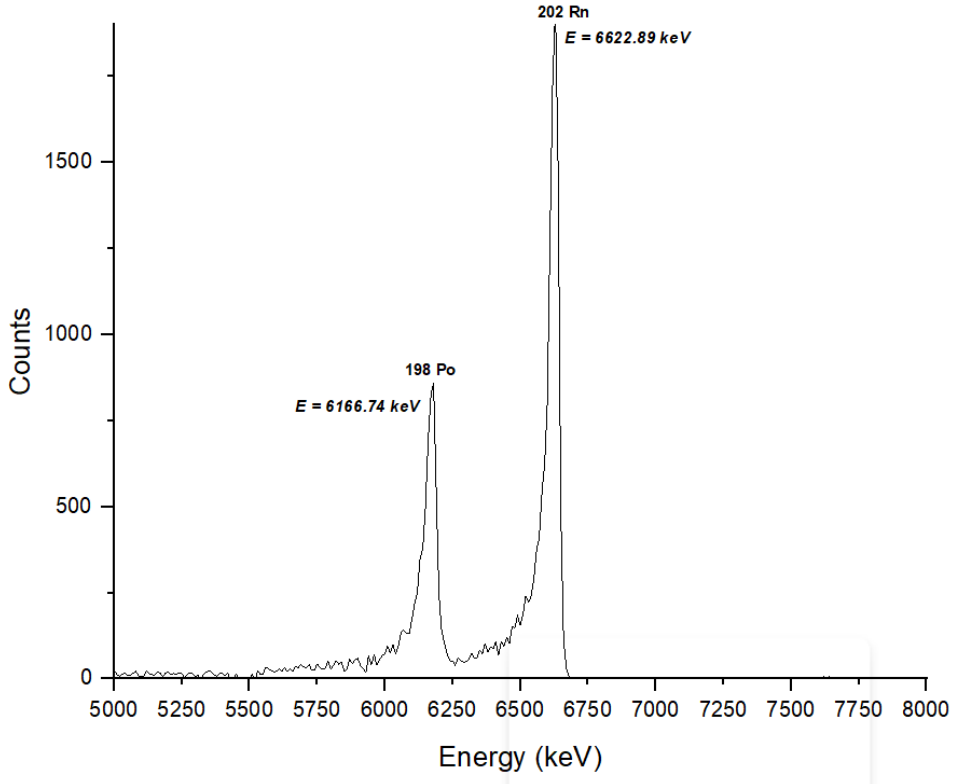

: 1D spectra of ^{202}Rn isotope

Peak Index	Peak Type	Area Intg	FWHM	Max Height	Center Grvty	Area IntgP
1	Gaussian	529.66006	52.02462	150.41041	6066.71659	0.69805
2	Gaussian	16376.07189	94.76967	196.20879	6508.97652	21.58239
3	Gaussian	58971.27161	25.39705	511.64135	6547.57869	77.71956

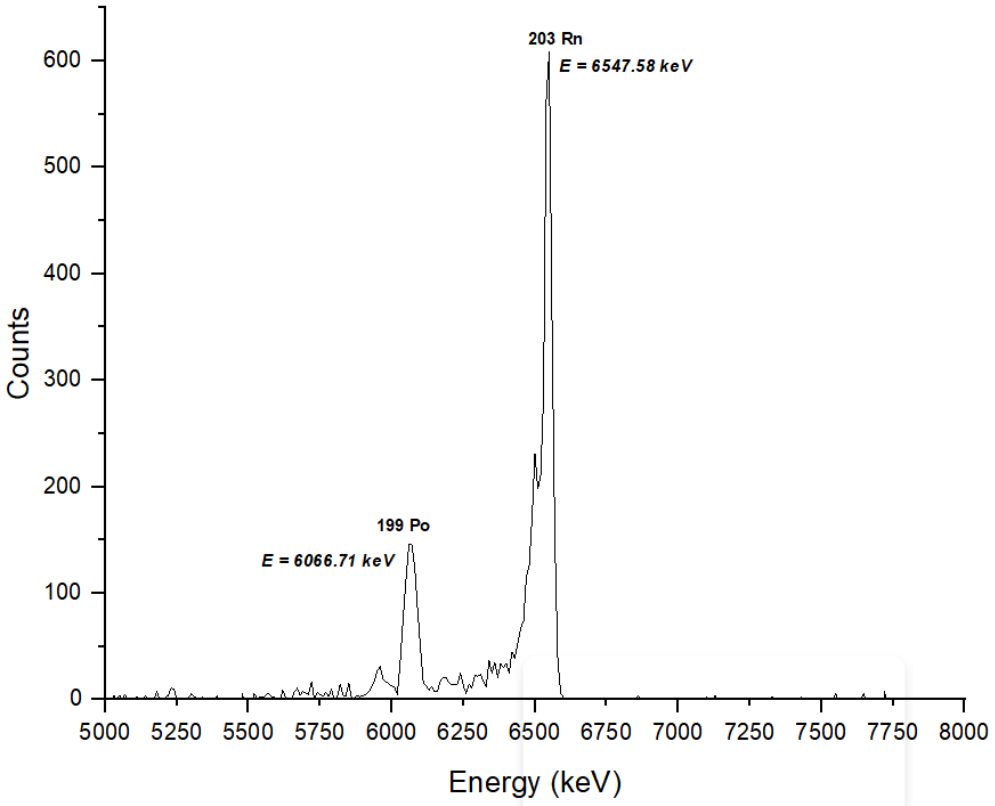

: 1D spectra of ^{203}Rn isotope

Peak Index	Peak Type	Area Intg	FWHM	Max Height	Center Grvty	Area IntgP
1	Gaussian	1.71277E-20	44.81736	189.25149	6395.34462	100

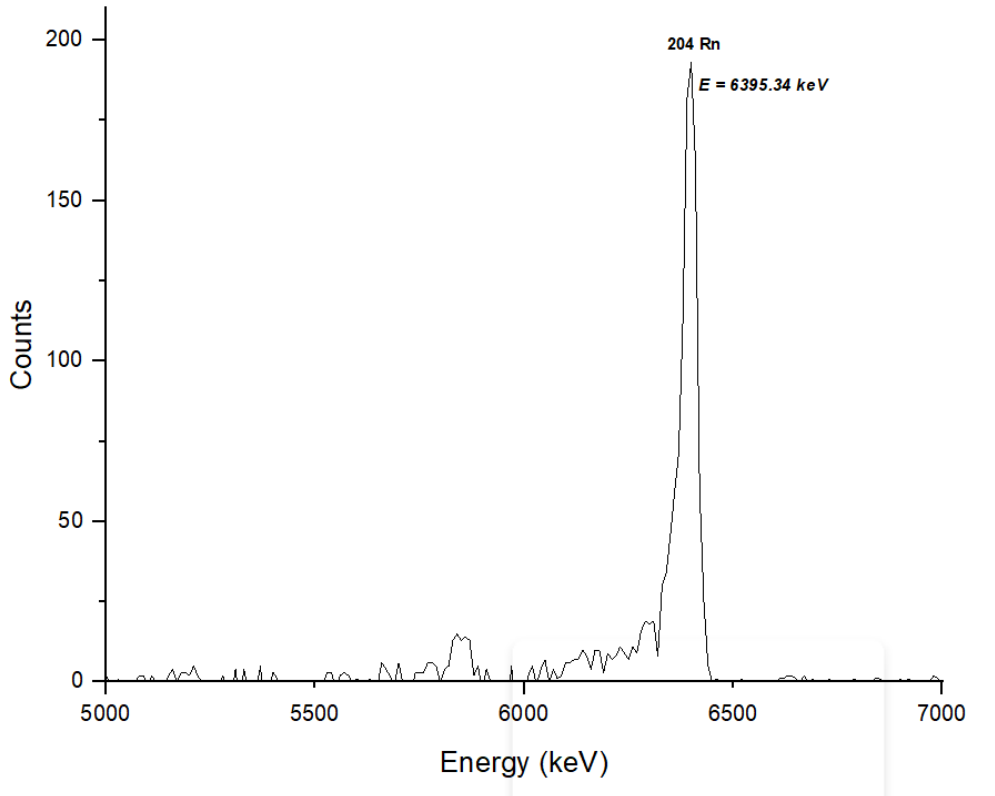

: 1D spectra of ^{204}Rn isotope

Peak Index	Peak Type	Area Intg	FWHM	Max Height	Center Grvty	Area IntgP
1	Gaussian	597.87945	46.15228	12.17299	5904.78247	8.39018
2	Gaussian	2243.94977	55.05883	38.28761	6260.78831	31.48988

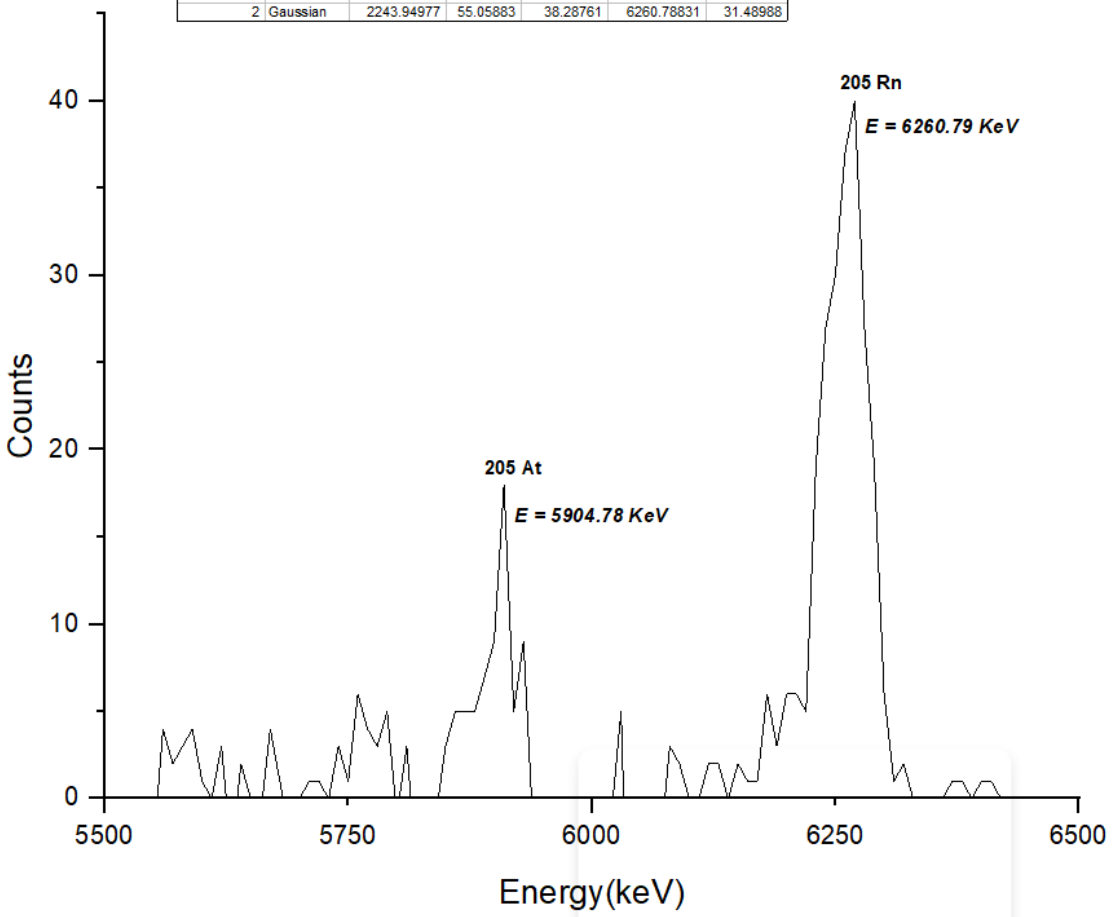

: 1D spectra of ^{205}Rn isotope

Heatmap of alpha decay energy of $^{40}Ar + ^{166}Er$-

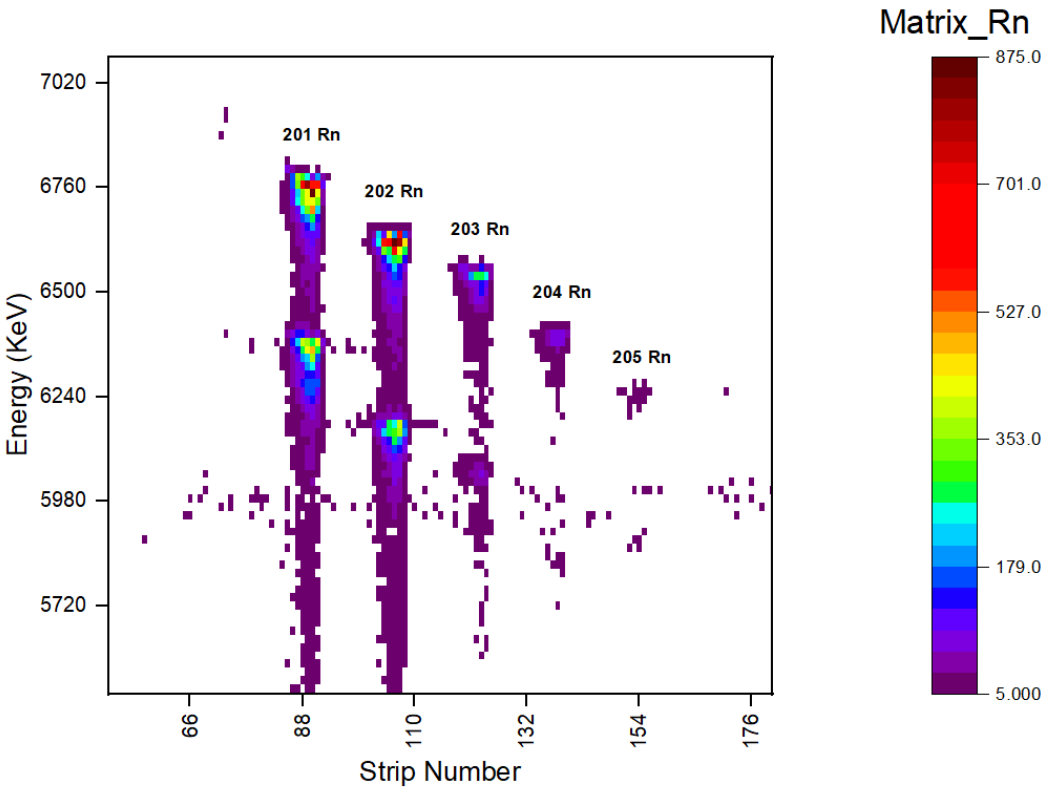

: 2D heatmap of alpha decay energies of $^{201\text{-}205}Rn$ isotopes

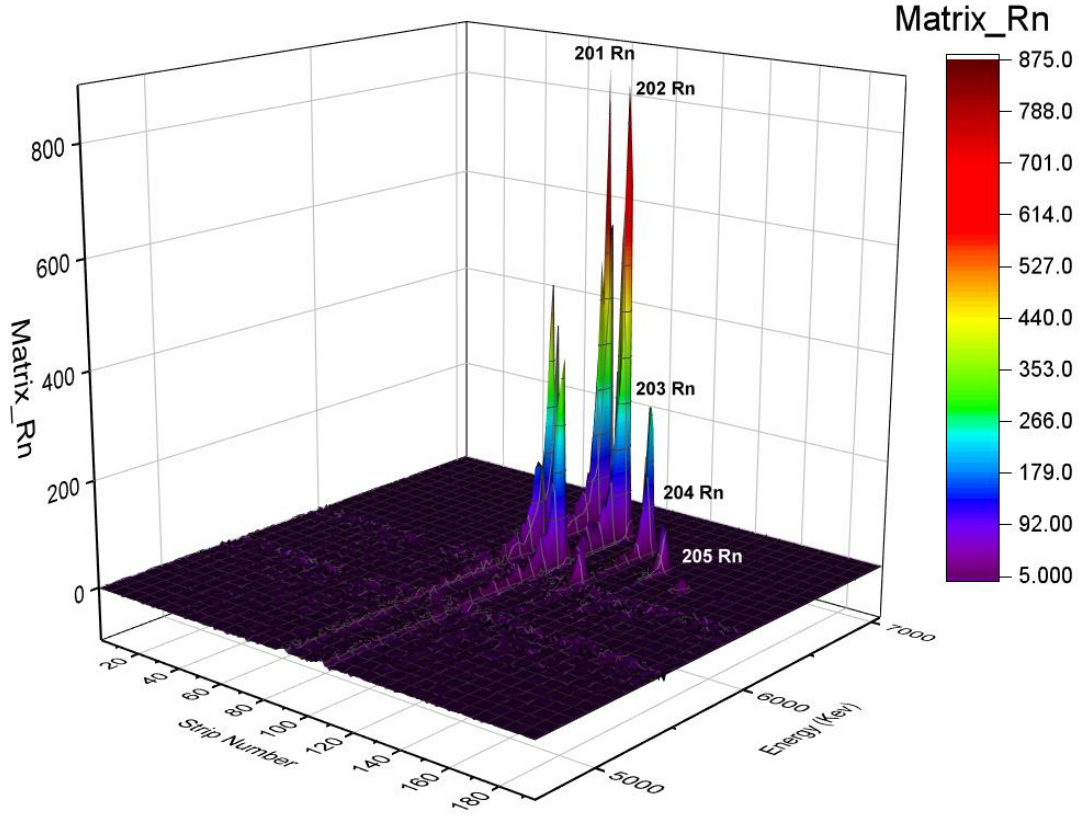

: 3D heatmap of alpha decay energies of $^{201\text{-}205}Rn$ isotopes

(iii) $^{48}Ca + ^{242}Pu$:

Peak Index	Peak Type	Area Intg	FWHM	Max Height	Center Grvty	Area IntgP
1	Gaussian	198900.80176	5.94651	10392.11743	6235.89599	100

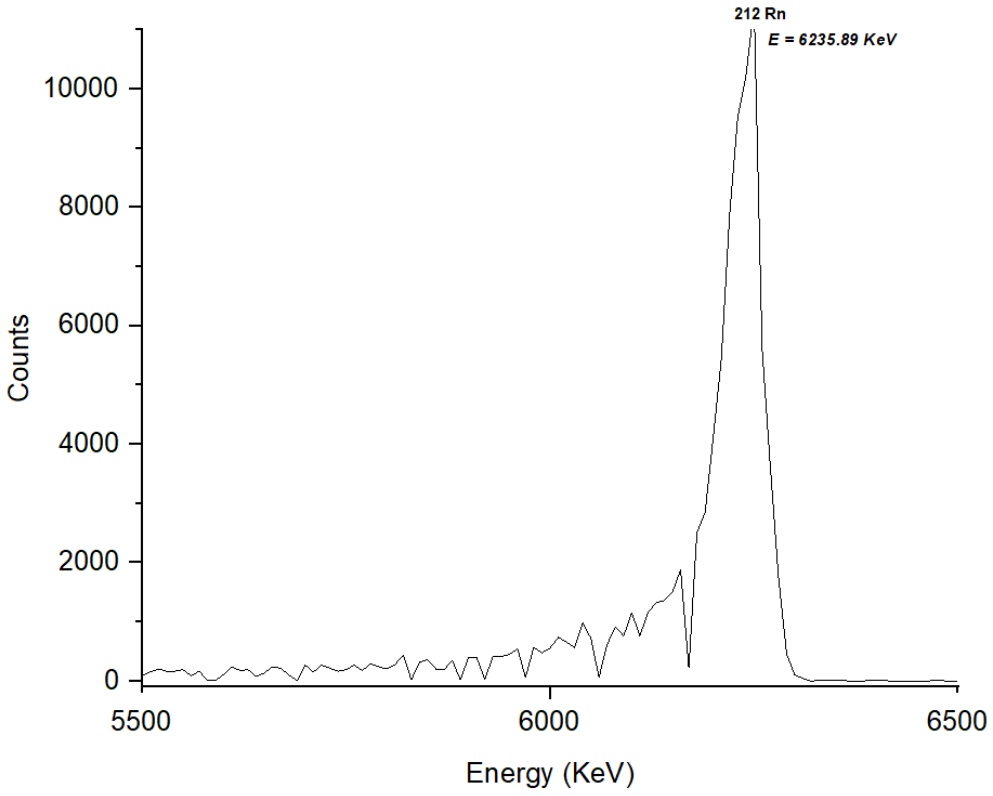

: 1D spectra of ^{212}Rn isotope

Peak Index	Peak Type	Area Intg	FWHM	Max Height	Center Grvty	Area IntgP
1	Gaussian	5.99854	0.62772	7.07417	5282.84419	1.44244
2	Gaussian	29.29094	3.5504	7.75041	6592.47157	7.04345
3	Gaussian	9.10348	1.38882	6.15819	7111.55507	2.18907
4	Gaussian	24.31114	3.21351	7.10718	7356.47989	5.84599
5	Gaussian	19.48775	4.3148	4.24297	7660.80777	4.68613

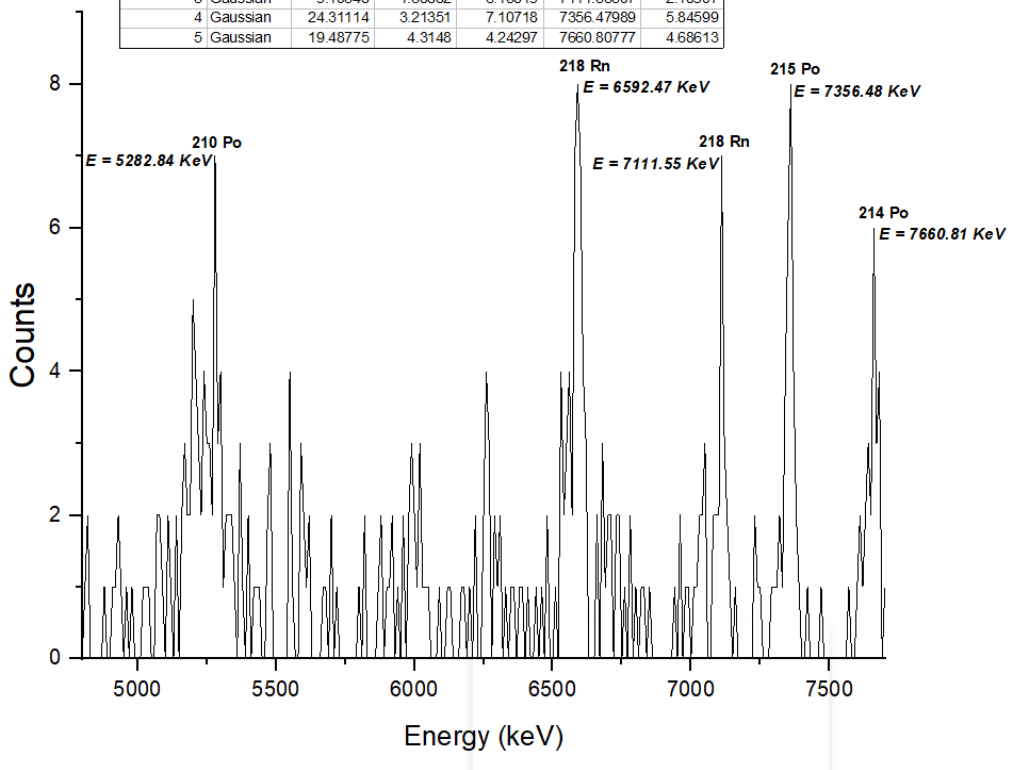

: 1D spectra of ^{218}Rn isotope

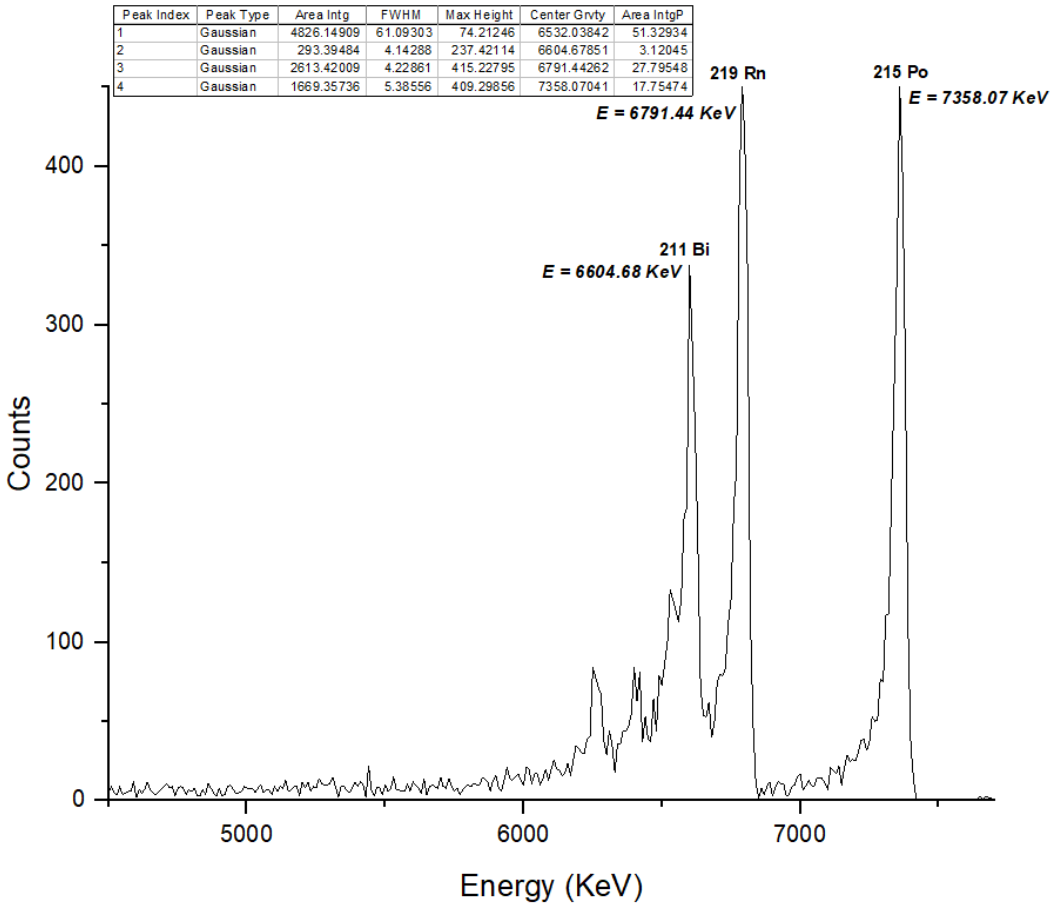

: 1D spectra of ^{219}Rn isotope

Heatmap of alpha decay energy of $^{48}Ca + ^{242}Pu$-

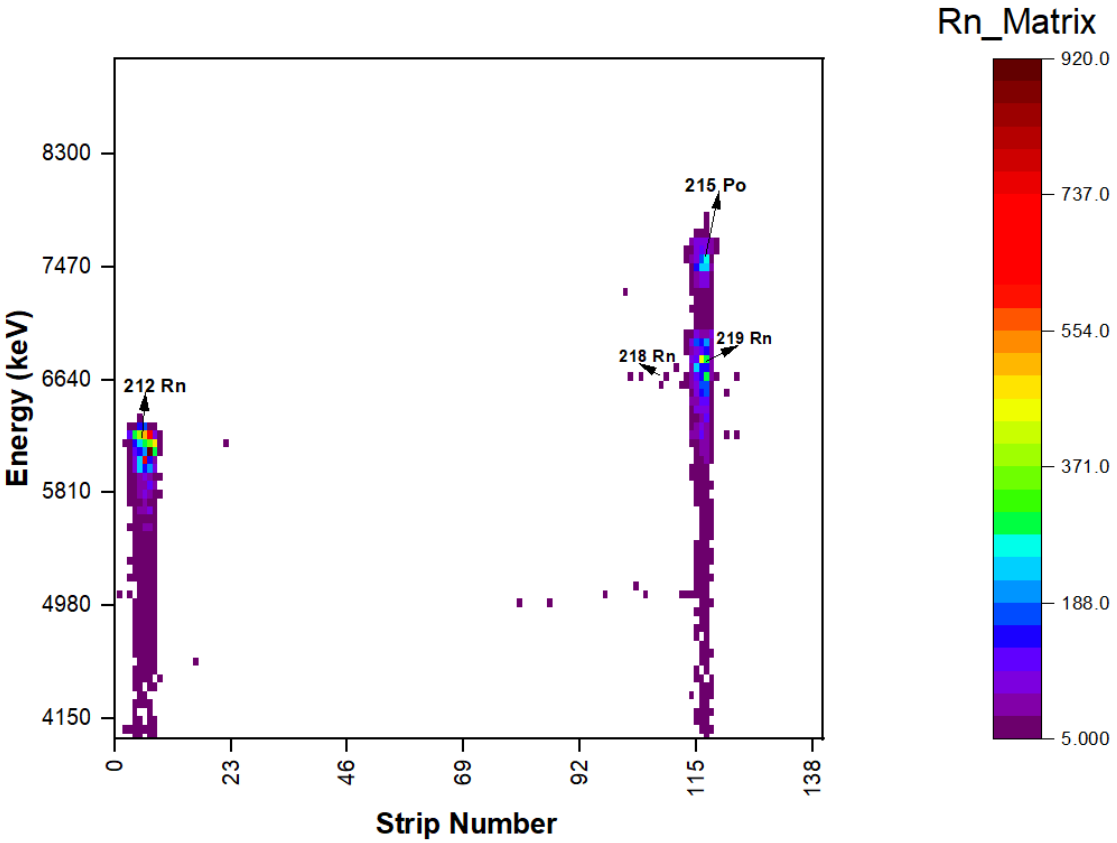

: 2D heatmap of alpha decay energies of $^{212,218\text{-}219}Rn$ isotope

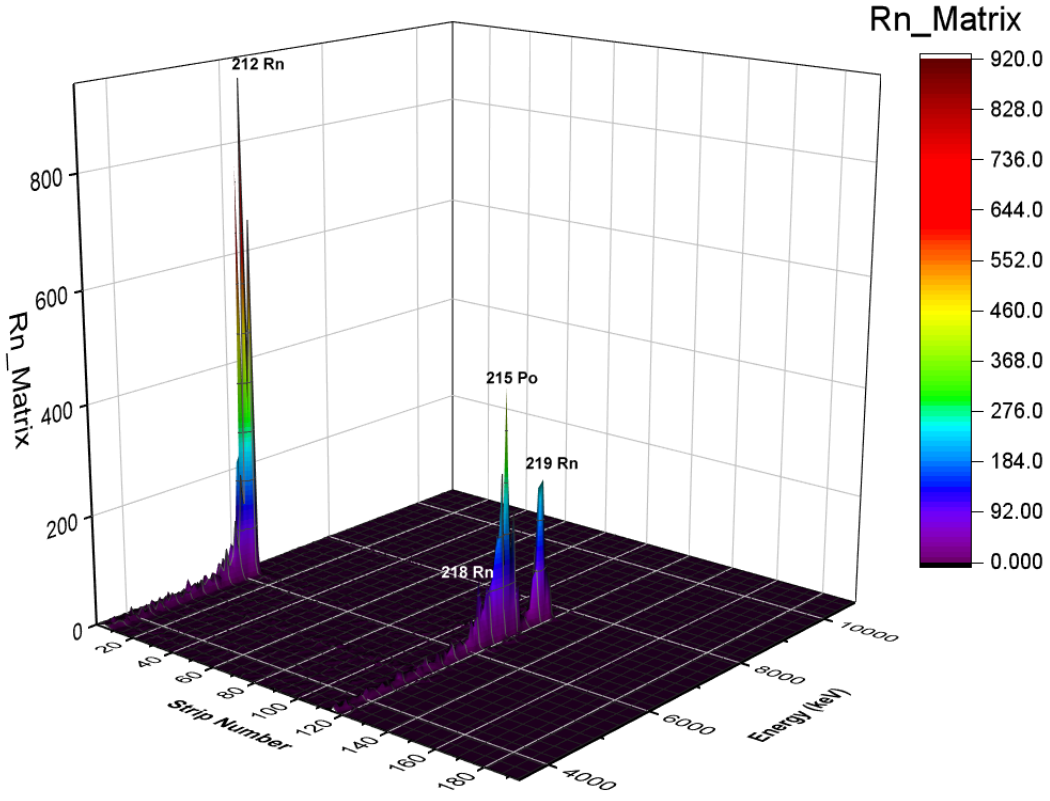

: 3D heatmap of alpha decay energies of $^{212,\ 218\text{-}219}Rn$ isotopes

Conclusion

The summarization of the above results is –

(i) $^{40}Ar + {}^{148}Sm \rightarrow {}^{180\text{-}185}Hg$

SL No.		Peak Alpha Decay Energy (keV)	Isotope Identification	Probability of specific isotope (%)
1	^{180}Hg	6122.73	^{180}Hg	99.87
		5728.59	^{176}Pt	99.74
2	^{181}Hg	5990.53	^{181}Hg	87.00
3	^{182}Hg	5855.61	^{182}Hg	99.00
4	^{183}Hg	7640.00	^{183}Hg	91.00
5	^{184}Hg	5531.76	^{184}Hg	99.44
6	^{185}Hg	5646.41	^{185}Hg	96.00

(ii) $^{40}Ar + {}^{166}Er \rightarrow {}^{201\text{-}205}Rn$

SL No.		Peak Alpha Decay Energy (keV)	Isotope Identification	Probability of specific isotope (%)
1	^{201}Rn	6745.94	^{201}Rn	100.00
		6374.38	^{197}Po	99.30
2	^{202}Rn	6622.89	^{202}Rn	99.99
		6166.74	^{198}Po	99.99
3	^{203}Rn	6547.58	^{203}Rn	100.00
		6066.71	^{199}Po	100.00
4	^{204}Rn	6395.34	^{204}Rn	-
5	^{205}Rn	6260.79	^{205}Rn	98.20
		5904.78	^{205}At	100.00

(iii) $^{48}Ca + {}^{242}Pu \rightarrow {}^{212,\ 218\text{-}219}Rn$

SL No.		Peak Alpha Decay Energy (keV)	Isotope Identification	Probability of specific isotope (%)
1	^{212}Rn	6235.89	^{212}Rn	99.95
2	^{218}Rn	5285.84	^{210}Po	100.00
		6592.47	^{218}Rn	0.13
		7111.55	^{218}Rn	99.87

		7356.48	^{215}Po	100.00
		7660.81	^{214}Po	99.99
3	^{219}Rn	6604.68	^{211}Bi	83.77
		6791.44	^{219}Rn	79.40
		7358.07	^{215}Po	100.00

Another observation that can be noted is that in the heatmap plot of ^{48}Ca + ^{242}Pu, the matrix for $^{213\text{-}217}$Rn does not exist. This can be explained by the significantly less half-life of these isotopes, i.e., of the order of 0.5 ms, while the response time of the solid ISOL method is about 1.8 s.

Acknowledgment

I am very much thankful to the JINR Interest training program for providing me with the opportunity to participate in this project. I give my special thanks to Mr. Viacheslav Vedeneev for his guidance throughout the project. This program has helped me explore my interest in accelerator physics, and I am looking further to future collaborations.

References

[1] Rodin, A. & Belozerov, A. & Vanin, D. & Vedeneyev, V. & Gulyaev, A. & Gulyaeva, A. & Dmitriev, Sergey & Itkis, M.G. & Kliman, J. & Kondratiev, N. & Krupa, L. & Oganessian, Yu & Salamatin, V. & Siváček, Ivan & Stepantsov, S. & Chernysheva, E. & Yuchimchuk, S.. (2014). MASHA separator on the heavy ion beam for determining masses and nuclear physical properties of isotopes of heavy and superheavy elements. Instruments and Experimental Techniques. 57. 386-393. 10.1134/S0020441214030208.

[2] Mamatova, Meruyert & Seitkali, Assylkan & Kudaibergenova, Eleonora & Rodin, Aleksandr & Krupa, L. & Chernysheva, E. & Vedeneev, Vyacheslav & Novoselov, Aleksey & Podshibyakin, Aleksandr & Salamatin, Vladimir & Stepantsov, Sergey & Gulyaev, Aleksandr & Yukhimchuk, Sergey & Komarov, Aleksandr & Kamas, Dusan & Opichal, Antonin & Kliman, J.. (2019). Study of production stability of radon and mercury isotopes in complete fusion reactions at the mass-separator MASHA by “solid hot catcher” technique. AIP Conference Proceedings. 2163. 070002. 10.1063/1.5130114.

[3] Vedeneev, V. & Rodin, A. & Krupa, L. & Belozerov, A. & Chernysheva, E. & Dmitriev, Sergey & Gulyaev, A. & Gulyaeva, A. & Kamas, D. & Kliman, J. &

Komarov, A. & Motycak, S. & Novoselov, A. & Salamatin, V. & Stepantsov, S. & Podshibyakin, A. & Yukhimchuk, S. & Granja, Carlos & Pospisil, Stanislav. (2017). The current status of the MASHA setup. Hyperfine Interactions. 238. 10.1007/s10751-017-1395-9.

[4] H. W. Gäggeler, “Mendeleev's principle against Einstein's relativity: news from the chemistry of superheavy elements”, Usp. Khim., 78:12 (2009), 1228–1233; Russian Chem. Reviews, 78:12 (2009), 1139–1144.

[5] Eichler, R., Aksenov, N., Belozerov, A. et al. Chemical characterization of element 112. Nature 447, 72–75 (2007). https://doi.org/10.1038/nature05761

[6] Rodin, A. & Chernysheva, E. & Dmitriev, Sergey & Gulyaev, A. & Kamas, D. & Kliman, J. & Krupa, L. & Novoselov, A. & Oganessian, Yu & Opichal, Antonin & Podshibyakin, A. & Salamatin, V. & Stepantsov, S. & Vedeneev, V. & Yukhimchuk, S.. (2020). Features of the Solid-State ISOL Method for Fusion Evaporation Reactions Induced by Heavy Ions. 437-443. 10.1142/9789811209451_0062.

[7] Chernysheva, E. & Rodin, A. & Dmitriev, Sergey & Gulyaev, A. & Komarov, A. & Novoselov, A. & Oganessian, Yu & Podshibyakin, A. & Salamatin, V. & Stepantsov, S. & Vedeneev, V. & Yukhimchuk, S. & Krupa, L. & Holik, Michael & Pospisil, Stanislav & Stekl, I. & Kliman, J. & Kamas, D. & Opichal, Antonin & Maher, A.. (2020). Determination of Separation Efficiency of the Mass-Spectrometer MASHA by Means of Measurement of Absolute Cross-Sections of Evaporation Residues. 386-390. 10.1142/9789811209451_0054.

[8] Dmitriev, Sergey & Ts, Yury & Oganessyan, & Utyonkov, Vladimir & Shishkin, Sergey & Yeremin, A. & Lobanov, Yury & Tsyganov, Yury & Chepygin, Viktor & Evgeny, Sokol & Vostokin, Grigory & Aksenov, Nikolay & Hussonnois, Michel & Itkis, M.G. & Gaeggeler, Heinz & Schumann, Dorothea & Bruchertseifer, Horst & Eichler, Robert & Shaughnessy, Dawn & Wild, John. (2004). Chemical identification of dubnium as a decay product of element 115 produced in the reaction ^{48}Ca + ^{243}Am. Mendeleev Communications.